Jurnal Teknologi

Full Paper

GELLAN GUM- AND PECTIN-MAGNETIC GRAPHENE OXIDE NANOCARRIERS LOADED WITH CINNAMALDEHYDE FOR MOSQUITO LARVAE CONTROL

Siew Tin Susana Wong[a], Azlan Kamari[a]*, Siti Najiah Mohd Yusoff[a], Mohd Zobir Hussein[b], Hidayatulfathi Othman[c], Suzaliza Mustafar[a], Adulsman Sukkaew[d], Is Fatimah[e]

[a]Department of Chemistry, Faculty of Science and Mathematics, Universiti Pendidikan Sultan Idris, 35900 Tanjong Malim, Perak, Malaysia
[b]Institute of Nanoscience and Nanotechnology, Universiti Putra Malaysia, 43400 Serdang, Selangor, Malaysia
[c]School of Diagnostic and Applied Health Sciences, Faculty of Health Sciences, Universiti Kebangsaan Malaysia, 50300 Kuala Lumpur, Malaysia
[d]Faculty of Science Technology and Agriculture, Yala Rajabhat University, 133 Thesaban 3, Sateng, Muang, Yala, 95000, Thailand
[e]Department of Chemistry, Faculty of Mathematics and Natural Sciences, Universitas Islam Indonesia, Jl. Kaliurang Km 14, Yogyakarta 55584, Indonesia

Article history
Received
12 April 2023
Received in revised form
18 October 2023
Accepted
28 November 2023
Published Online
18 February 2024

*Corresponding author
azlan.kamari@fsmt.upsi.edu.my

Graphical abstract

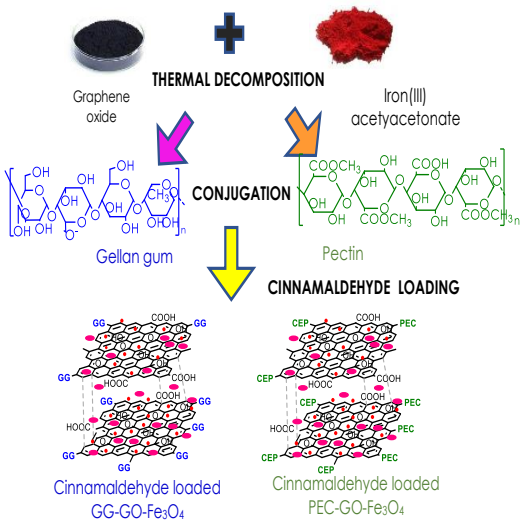

Abstract

Magnetic nanoparticles have evolved over the last few decades as nanocarriers in drug delivery systems for hydrophobic drugs. Here, novel gellan gum magnetic graphene oxide (GG-GO-Fe_3O_4) and pectin magnetic graphene oxide (PEC-GO-Fe_3O_4) nanocomposites were prepared to carry cinnamaldehyde to control *Aedes aegypti* larvae. Fourier transform infrared (FTIR) spectroscopy, field emission scanning electron microscopy (FESEM) and scanning transmission electron microscopy (STEM) were employed to investigate the physicochemical characteristics of the nanocomposites. Entrapment efficiencies and loading capacities of nanocomposites on cinnamaldehyde were examined using ultraviolet-visible analysis. The successful cinnamaldehyde loading was confirmed by C-C and C-O stretches in the FTIR spectra. Results of *in vitro* release study showed the capabilities of GG-GO-Fe_3O_4 as a drug carrier system, extending the cinnamaldehyde release period for 36 h, and the release profiles for both nanocomposites fit the Korsmeyer-Peppas kinetic model with correlation coefficient (R^2) values of over 0.9809. The cinnamaldehyde-loaded GG-GO-Fe_3O_4 nanocomposites induced 68% mortality after 72 h of exposure, with LC_{50} values ranging from 2.0488 and 15.9121 mg/L. The conjugation of GO-Fe_3O_4 with biopolymers improved the water solubility of cinnamaldehyde by 36.41 to 62.83 times vs. free cinnamaldehyde in water (1.42 mg/mL). Overall, these results are beneficial for researchers dealing with mosquito control and prevention.

Keywords: *Aedes aegypti*, cinnamaldehyde, gellan gum, magnetic nanocarrier, pectin

Abstrak

Nanozarah magnetik telah berkembang sebagai nanopembawa dalam sistem penghantaran ubat untuk ubat hydrophobia sejak beberapa dekad lalu. Di sini, nanokomposit gam gellan grafin oksida magnetik (GG-GO-Fe_3O_4) dan pectin grafin oksida magnetik (PEC-GO-Fe_3O_4) baru telah disediakan untuk membawa sinamaldehid bagi mengawal jentik-jentik *Aedes aegypti*. Spektroskopi inframerah transformasi Fourier (FTIR), mikroskopi pengimbas elektron pancaran medan (FESEM) dan mikroskopi pengimbas penghantaran elektron (STEM) telah digunakan untuk mengkaji sifat fizikokimia nanokomposit. Keberkesanan pemerangkapan dan keupayaan muatan nanokomposit telah diperiksa melalui analisis ultralembayung-nampak. Kejayaan muatan sinamaldehid telah disahkan dengan keregangan C-C dan C-O dalam spektra FTIR. Keputusan daripada kajian lepasan *in vitro* menunjukkan keupayaan GG-GO-Fe_3O_4 sebagai sistem pembawa ubat, memanjangkan tempoh pelepasan sinamaldehid selama 36 jam, dan profil pelepasan untuk kedua-dua nanokomposit disesuaikan dengan model kinetik Korsmeyer-Peppas dengan nilai pekali korelasi (R^2) melebihi 0.9809. GG-GO-Fe_3O_4 yang telah dimuatkan dengan sinamaldehid menyebabkan 68% kematian selepas 72 jam pendedahan, dengan nilai LC_{50} berjulat daripada 2.0488 ke 15.9121 mg/L. Konjugasi antara GO-Fe_3O_4 dengan biopolimer meningkatkan kelarutan air bagi sinamaldehid dengan 36.41 ke 62.83 kali ganda daripada sinamaldehid bebas dalam air (1.42 mg/L). Keseluruhannya, semua keputusan ini bermanfaat kepada penyelidik yang berurusan dengan pengawalan dan pencegahan nyamuk.

Kata kunci: *Aedes aegypti*, gam gellan, pektin, nanopembawa magnetic, sinamaldehid

1.0 INTRODUCTION

The high proliferation rates and number of deaths caused by mosquito-borne diseases have raised many concerns from the public around the world [1]. According to the World Health Organization [2], 50% of the world population are exposed to the risk of dengue infection and 100-400 million infections are estimated to occur per year. Furthermore, global dengue infection cases increased nearly 8-fold over two decades, with approximately 70% of cases in Asia. The Southeast Asia and Western Pacific regions are those most affected by dengue [2]. In the year of 2023, there were 25,248 dengue cases reported in the Philippines and 2,123 dengue cases recorded in Singapore [3]. In addition, Sri Lanka recorded 12, 496 dengue cases from January 1st to March 3rd, 2023 [4]. Hence, the vector of infection should be reduced in order to control the proliferation of disease.

The warm climate and high humidity are important factors which induce high mosquito breeding rates [5], especially in Malaysia, Thailand and Indonesia. In order to reduce the mosquito population and the main vector contact, chemical and biological control methods are combined in combating mosquito breeding sites and biting activities. Larval source management is applied to observe mosquito population density changes [6]. *A. aegypti* and *A. albopictus* are the two main dengue vectors that lay eggs in households and artificial containers. The mobility of larvae is only in water, and this makes reducing the breeding sites of larvae much easier than reducing the habitats of adults.

In the current market, several forms of larvicides such as liquids, pellets, tablets and granules are available. Larvicide formulations are categorised into three types, namely: (1) bacterial, (2) insect growth regulators, and (3) oils or films. However, these face certain drawbacks such as low solubility and high toxicity towards non-target species upon their application, especially for the oils or films–type. After application of the oils and films–type larvicide in water a thin layer of oil forms on the water's surface, and this will block air from entering water. This has a significant effect on aquatic organisms. The application of oils and films–type larvicides, which are synthetic materials, is not favourable in this context.

In recent years, several plant extracts have been used as larvicide formulations, such as peppermint, betel and lavender. In this study, cinnamaldehyde, an essential oil extracted from cinnamon bark, has been used in larvicide formulation. Cinnamaldehyde makes up nearly 82% of the essential oil of cinnamon bark and is the most abundant among its components. Cinnamaldehyde is the compound that gives cinnamon its flavour and odour. Its scientific name is 3-phenylprop-2-enal. Cheng and co-workers [7] reported that cinnamaldehyde coexhibited great abilities to control mosquito larvae over 24 h. However, cinnamaldehyde is only slightly soluble in water (1.42 mg/mL at 25 °C) and it takes time to diffuse into water in order to kill mosquito larvae. Thus, a drug delivery

system is necessary to carry cinnamaldehyde into a water environment.

Drug delivery systems are formulations that introduce drugs into an environment or body in order to increase their efficacy and safety by controlling the release rate or location. Application of polysaccharides has only recently become a trend in drug delivery, despite their distinct advantages such as hydrophilicity, non-toxicity, biodegradability, low-cost and abundance. Numerous studies reported that modification of polysaccharides leads to sustained release of drugs for a longer period of time. For instance, Wong *et al*. [8] proposed a sodium alginate-chitosan nanocomposite for carrying cinnamaldehyde, and this system offered a high entrapment efficiency of cinnamaldehyde (95.25%).

In this study, a magnetic nanocarrier system is developed to carry cinnamaldehyde into water in order to reduce mosquito larvae. Conjugation of gellan gum and pectin with magnetised graphene oxide (GO-Fe_3O_4) is beneficial for cinnamaldehyde entrapment and loading. The release profiles of cinnamaldehyde from the magnetic nanocomposites into rainwater and their potential to control *A. aegypti* larvae were investigated in detail.

2.0 METHODOLOGY

2.1 Materials

Iron acetylacetonate ($Fe(C_5H_7O_2)_3$, purity 99+%), high-methoxyl PEC produced from apple (60–71% degree of esterification, molecular weight 130,000 g/mol) and triethylene glycol ($C_6H_{14}O_4$, purity 99%) were supplied by Thermo Scientific. GO sheets (purity 99%), high-acyl GG (50% degree of acylation, molecular weight 1,000,000 g/mol), and analytical standard cinnamaldehyde were supplied by Sigma Aldrich.

2.2 Preparation of GO-Fe_3O_4 Nanocomposites

The GO-Fe_3O_4 is prepared based on the method outlined by Hussien *et al.* [9], with some modifications. This process entails the dispersion and sonication of GO sheets (50 mg) in $C_6H_{14}O_4$ (200 mL) for 5 h. An exact amount of $Fe(C_5H_7O_2)_3$ (200 mg) was poured into the GO dispersion for another 45 min of sonication. Prior to gradually heating the dispersion, an argon-purged round bottom flask was prepared to remove any impurities. The dispersion was heated at 278 °C under an argon gas atmosphere for 50 min, then allowed to cool at room temperature (25 ± 1 °C) and let stand for 24 h. The nanocomposites were separated from the dispersion using a magnet and rinsed several times with ethanol (95%) and deionised water. Following the separation of nanocomposites, the drying process was performed in an oven at 70 °C for 3 h.

2.3 Conjugation of GO-Fe_3O_4 Nanocomposites with GG and PEC

A simple mixing procedure was applied in order to conjugate GG with GO-Fe_3O_4 nanocomposites. The first step involved mixing of GG (20 mL; 0.5 ppm in ultrapure water) and GO-Fe_3O_4 (20 mL; 1 ppm in PBS solution) in a centrifuge tube (50 mL). Then, the mixture underwent vortex treatment (1 min) and stirring (24 h, 100 rpm) at room temperature (24 ± 1 °C). The GG-GO-Fe_3O_4 nanocomposites were gently collected using a magnet, rinsed with deionised water and finally air-dried. A similar procedure was used to prepare PEC-GO-Fe_3O_4 nanocomposites.

2.4 Cinnamaldehyde Loading into Nanocomposites

To load cinnamaldehyde into the nanocomposites in a 1:5 ratio (v/w), cinnamaldehyde (1 mL) was added to 5 mg of nanocomposites in acetonitrile for 24 h and stirred at 100 rpm at 24 ± 1 °C. The cinnamaldehyde-loaded nanocomposites were dried out on a heating mantle under the temperature condition kept near 200 °C until completely dry. This optimum temperature was selected because it is ideal to dry free cinnamaldehyde from the drug carrier system and to prevent aggregation [10]. The dried cinnamaldehyde-loaded nanocomposites can be stored in granule form for further analysis.

The prepared nanocomposites were kept in air-tight containers at room temperature. An identical approach was carried out using ratios of 1:15 (v/w) and 1:25 (v/w) by increasing the mass of nanocomposites.

2.5 Characterisation Studies

2.5.1 Magnetisation

Magnetic characterisation was performed at 24 ± 1 °C using a Lake Shore 7404 vibrating sample magnetometer (VSM) set at applied magnetic field of ±15,000 Gauss. Samples were placed inside detection coils and exposed to magnetic vibration. During the analysis, the voltage change in the detecting coils was caused by the magnetic moment of the sample. The maximum magnetisation values for GO-Fe_3O_4, GG-GO-Fe_3O_4 and PEC-GO-Fe_3O_4 were determined as 13.21, 11.65 and 9.34 emu/g, respectively.

2.5.2 FTIR

FTIR analysis was conducted using a IRTracer-100 Shimadzu FTIR Spectrometer equipped with an attenuated total rays (ATR) component. A small amount of sample was positioned on the diamond surface. The samples were recorded at instrument settings of wavenumber (4000–400 cm^{-1}), number of scans (32) and resolution (8 cm^{-1}).

2.5.3 FESEM

Prior to surface morphology analysis, a platinum coating was applied on the sample in order to provide a conductive layer to prevent charging effects. A Hitachi SU 2020 Ultra High Resolution (UHR) FESEM was used for this study. The image of surface texture of the

samples was captured at several magnifications under acceleration voltages ranging from 1 to 30 kV.

2.5.4 STEM

A Hitachi SU 2020 UHR FESEM was used to observe the internal texture of nanocomposites at 100,000× magnification. In this study, methanol (2.0 mL) was used to disperse nanocomposites (10.0 mg) for sonication in a Branson Ultrasonic Cleaner CPX 1800-J for 30 min. Following sonication, approximately two drops of sample solution were deposited on a copper grid (carbon-coated; 300-mesh) and air-dried on filter paper at 25 ± 1 °C to remove excess solution. A tungsten filament was used as an electron emitter and the STEM analysis was carried out at 30.0 kV.

2.6 Cinnamaldehyde-Loading Studies

The cinnamaldehyde-loading studies were evaluated in terms of percentages for entrapment and loading at three different volume-to-weight ratios (cinnamaldehyde:nanocomposites): 1:5, 1:15, and 1:25. The amounts of encapsulated cinnamaldehyde were determined by UV-Vis analysis by measuring the absorbance percentage of the characteristic peak of the drug. The standard solutions were prepared using standard dilution methods and the concentration range was between 1 to 50 ppm. The calibration curves of absorbance versus wavelength were plotted. The maximum (λ) was determined as 298 nm. The formulae below were used to determine the entrapment (%) and loading (%) values [11]:

$$\text{Entrapment (\%)} = \frac{\text{Mass of cinnamaldehyde in the nanocomposite}}{\text{Mass of cinnamaldehyde initially loaded}} \times 100$$

$$\text{Loading (\%)} = \frac{\text{Mass of cinnamaldehyde in the nanocomposite}}{\text{Mass of nanocomposite}} \times 100$$

2.7 Cinnamaldehyde Release Studies

Cinnamaldehyde release experiments were carried out *in vitro* using rainwater collected in Tanjong Malim, Perak (pH = 5.55–5.84). In a 100 mL beaker, rainwater (50 mL) was added to cinnamaldehyde-loaded GG-GO-Fe_3O_4 (20 mg) and stirred at 100 rpm. At every interval of 1 h, 10 mL of sample solution was pipetted out and the same amount of freshly collected rainwater was added to maintain the same sink condition. An Agilent Cary 60 UV-visible spectrophotometer set at a wavelength of 298 nm was used to determine the amount of cinnamaldehyde released. The study was conducted in three replicates and standard deviations for each set of study were calculated.

In this study, the release behaviour of cinnamaldehyde from the GG-GO-Fe_3O_4 and PEC-GO-Fe_3O_4 nanocomposites was investigated using four kinetic models, namely: (1) zero-order ($Q_o - Q_t = K_o t$); (2) first-order ($dc/dt = -Kc$); (3) Higuchi model ($Q = A\sqrt{D(2C - C_s)C_s t}$); (4) Korsmeyer-Peppa model ($M_t/M_f = kt^n$). The graph of each equation was plotted and R^2 values were determined. The release exponent (n) for the Korsmeyer-Peppas model was computed using regression analysis [12]. Abbreviations for the equations are listed as below:

- Q_o Initial amount of cinnamaldehyde
- Q_t Cumulative amount of cinnamaldehyde release at time t
- c Concentration of cinnamaldehyde in the nanocomposite
- K_o Zero-order release constant
- K First-order release constant
- Q Amount of cinnamaldehyde release in time t per unit area A
- C Initial concentration of cinnamaldehyde
- C_s Solubility of cinnamaldehyde in the matrix media
- D Diffusion coefficient of cinnamaldehyde molecules in the matrix media
- M_t Amount of cinnamaldehyde release at time t
- M_f Maximum amount of cinnamaldehyde release
- *k* A constant indicating the release rate of cinnamaldehyde from the nanocomposite
- *n* Release exponent of cinnamaldehyde

2.8 Larvicidal Studies

The efficacy of cinnamaldehyde-loaded nanocomposites in controlling *A.aegypti* larvae was evaluated and compared with a common larvicide available on the market. The approval of animal research ethics (Ref. No. 2021-0008-15) was obtained from Research Ethics Committee of Universiti Pendidikan Sultan Idris, prior to conduct larvicidal studies. A plastic tray with a rectangular shape and capacity of 4200 cm^3 was used to rear the mosquito larvae. The rearing process was set up at a research laboratory of Biomedical Science, Universiti Kebangsaan Malaysia. The dose-response relationship was investigated by exposing freshly-ecdysed 4th instar larvae to cinnamaldehyde-loaded nanocomposites at three volume-to-weight ratios of 1:5, 1:15 and 1:25. In addition to cinnamaldehyde-loaded nanocomposites, a toxicity control test was also conducted by using cinnamaldehyde-unloaded nanocomposites. The purpose of this toxicity control test was to evaluate the possible toxicity of nanocomposites.

For a comparative study, 30 mg of cinnamaldehyde-loaded nanocomposites were prepared. Commercial larvicide (2 g) was dissolved in deionised water (1 L). Sample cups containing 25 mL of rainwater (pH = 5.55–5.84) and ten larvae were mixed with cinnamaldehyde-loaded nanocomposites (20 mg) or commercial larvicide solution (5 mL). The effect of larvicide on mosquito larvae was monitored

over 72 h exposure time. The experiment was conducted in triplicate and rainwater was used as negative control.

Abbott's formula (Equation 3) was used to determine the percentage of mortality, while the median lethal concentration (LC_{50}) of cinnamaldehyde was computed through log Probit analysis (Equation 4). The Finney's table was used to obtain Probit values and the abbreviations in the equation are stated below [13].

$$\text{Mortality (\%)} = \frac{\text{Number of dead mosquito larvae}}{\text{Total number of mosquito larvae}} \times 100$$

$$P = \alpha + \beta\,[\log 10\ (\text{dose})]$$

P Probit (5 + inverse normal transform of the response rate)
α y-intercept of the graph
β Slope of the graph

3.0 RESULTS AND DISCUSSION

3.1 Characterisation Studies

3.1.1 FTIR

The FTIR spectra of GG-GO-Fe_3O_4 before and after loading with cinnamaldehyde are presented in Figure 1. According to Ganguly and Pramanik [14], the band at 3548 cm^{-1} in Figure 1(a) is attributed to O-H stretch. Meanwhile, bending vibrations for the water molecules absorbed on the nanocomposite are represented by the peak at 1618 cm^{-1}. The band at 1077 cm^{-1} can be assigned to C-O stretching vibrations in GG. The occupation of iron at tetrahedral and octahedral positions causes stretching vibrations of Fe-O, which led to the appearance of an absorption band at 660 cm^{-1}. In Figure 1(b), the broad peak at 3358 cm^{-1} represents the -OH groups in the nanocomposites following the entrapment of cinnamaldehyde. The characteristic peaks emerging within the region of 1766–1576 cm^{-1} may be due to the stretches of C=O in cinnamaldehyde or C=C between cinnamaldehyde and GG-GO-Fe_3O_4. The C-O stretching vibration from aryl ether between cinnamaldehyde and graphene oxide causes the peak at 1252 cm^{-1} to arise. It is interesting to note that the stretching vibration for Fe-O shifted from 660 to 697 cm^{-1} after entrapment of cinnamaldehyde, and this may be caused by a reduction in bond length between molecules or changes in electronegativity of neighbouring atoms [15, 16].

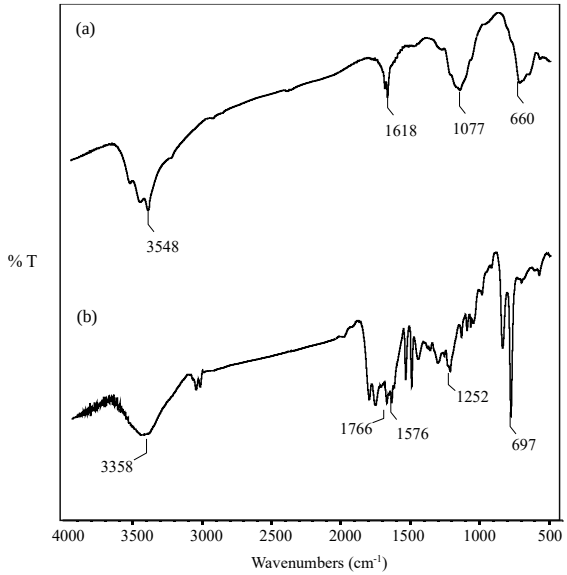

Figure 1 FTIR spectra of (a) GG-GO-Fe_3O_4 and (b) cinnamaldehyde loaded GG-GO-Fe_3O_4

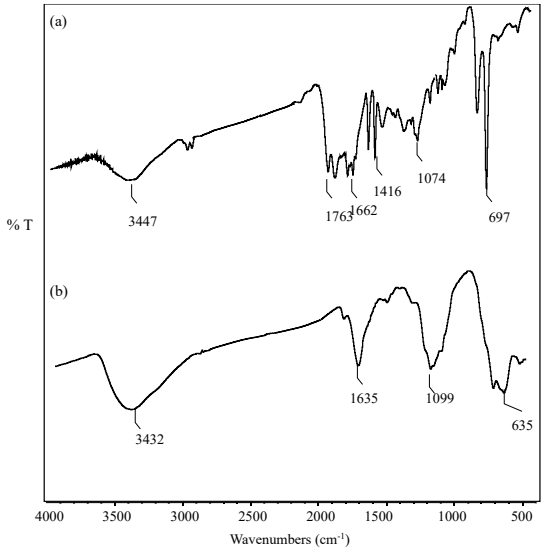

Figure 2 FTIR spectra of (a) PEC-GO-Fe_3O_4 and (b) cinnamaldehyde loaded PEC-GO-Fe_3O_4

Figure 2 presents the FTIR spectra of PEC-GO-Fe_3O_4 and cinnamaldehyde-loaded PEC-GO-Fe_3O_4. As depicted in Figure 2, the stretching vibrations of Fe-O were observed within the absorption bands range of 697–635 cm^{-1}. In Figure 2(a), the peaks at 3447 and 1763 cm^{-1} indicate O-H and C=O stretches. The absorption band at 1662 cm^{-1} corresponds to the scissoring vibration of O-H bonds in absorbed water molecules on the surface of the nanocomposites. In addition, the presence of glycosidic linkage between two galacturonic sugar are proven by the -OH bending in the alcohol at 1416 cm^{-1}, the -CH_2- bending vibration at 1662 cm^{-1}, and the discernible peak at 1074 cm^{-1}. When PEC-GO-Fe_3O_4 was loaded with cinnamaldehyde, the broad O-H stretching peak can be observed near 3432 cm^{-1}, as shown in Figure 2(b). Those absorption peaks at 1635 and 1099 cm^{-1}

could be assigned to C=C and C-O from cinnamaldehyde, respectively.

3.1.2 FESEM

In this study, any changes occurred on the surface of nanocomposites following cinnamaldehyde loading was investigated using FESEM. After conjugation with GG, the nanoparticles exhibited an appearance similar to coral-like deposits, as illustrated in Figure 3. This is in accordance to the findings from Balachandramohan *et al.* [17] who synthesised a Fe_3O_4-guar gum composite for the reduction of *p*-nitroaniline. Although the nanocomposites were synthesised via a sonochemical method, the morphology of the nanocomposites were cubic, round or plate-like after coating with GG. Their results indicated that the improved dispersion and reduced aggregation of particles were likely due to GG weakening the magnetic interaction between particles. In the case of PEC, the GO-Fe_3O_4 shows a cubic-like structure deposited on the surface. As depicted in Figure 3(b), the nanoparticles sink onto the surface of the porous structure. This phenomenon is due to the large defined area and high interfacial free energy of the nanoparticles. This is supported by the work of Ganguly and Pramanik [14].

Spherical nanocomposites are observed following cinnamaldehyde loading into GG-GO-Fe_3O_4 (Figure 3(c)). Meanwhile, aggregation can be observed, in accordance with findings by Zhu *et al.* [18], where the entrapment of cinnamaldehyde by chitosan hydrochloride/sulfobutyl ether cyclodextrin nanoparticles resulted in a coarse, fluffy, irregular surface. The PEC-GO-Fe_3O_4 nanocomposite presents a wrinkled structure after cinnamaldehyde is introduced into the system (Figure 3(d)), where the nanocomposites are aggregated and dispersed on the surface. PEC adsorption on the particles and the entrapment of particles by PEC gel results in large aggregations, and this may be caused by PEC network expansion at low ionic strengths or by steric hindrance of the chains [18, 19].

3.1.3 STEM

The internal morphology of nanocomposites was studied by means of STEM analysis. In Figure 4, the near-spherical shape of the magnetic nanoparticles can be observed. After introduction of GO-Fe_3O_4 into GO solution, GO-Fe_3O_4 nanocomposites remain on the surface of GO and are homogenously distributed. As depicted in Figure 4(a), after coating with GG, the GO-Fe_3O_4 nanocomposites have an irregular shape and are agglomerated into larger nanoparticles with size of around 65.5 to 121 nm, as the nanocomposites become surrounded by polysaccharide. The shape and size range of nanocomposites obtained from this study are in line with those reported by Ghibaudo *et al.* [20].

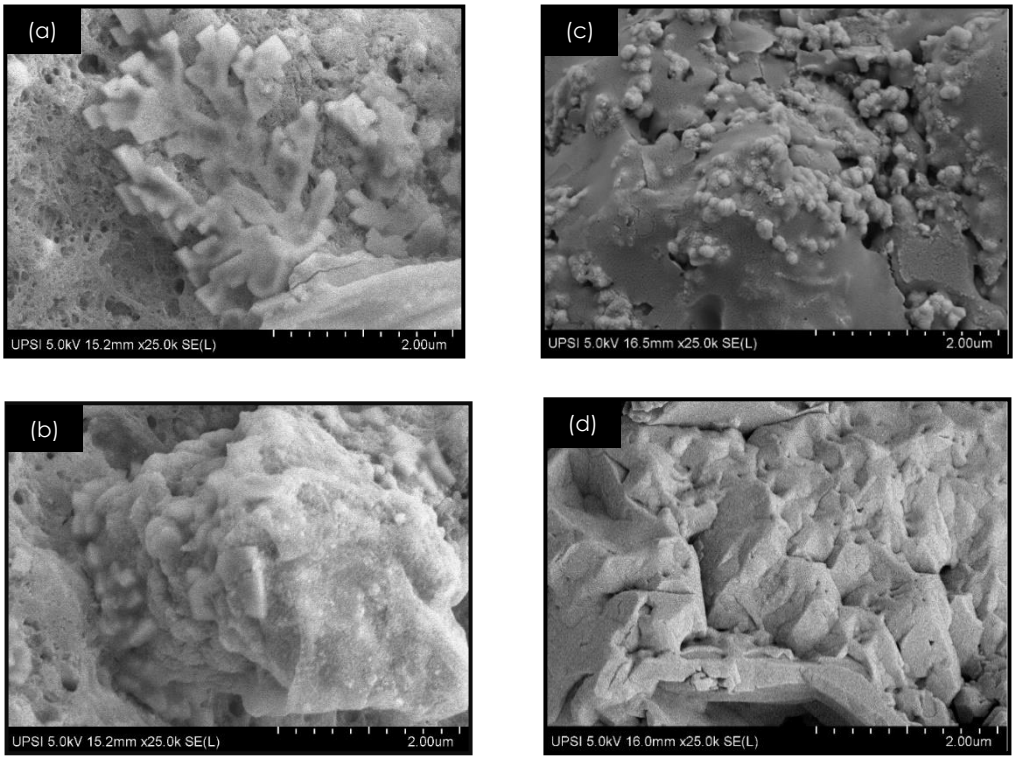

Figure 3 FESEM images of (a) GG-GO-Fe_3O_4, (b) PEC-GO-Fe_3O_4, (c) cinnamaldehyde loaded GG-GO-Fe_3O_4 and (d)cinnamaldehyde loaded PEC-GO-Fe_3O_4 at 25,000× magnification

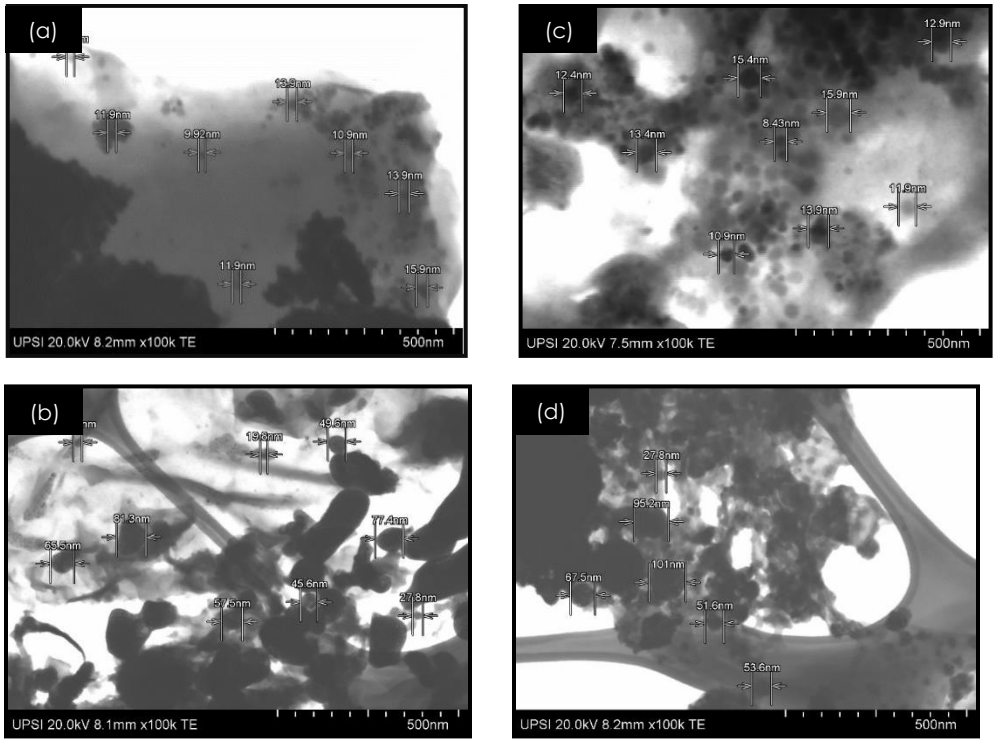

Figure 4 STEM images of (a) GG-GO-Fe_3O_4, (b) cinnamaldehyde loaded GG-GO-Fe_3O_4, (c) PEC-GO-Fe_3O_4 and (d) cinnamaldehyde loaded PEC-GO-Fe_3O_4 at 100,000× magnification

Figure 4(b) shows the internal morphology of cinnamaldehyde-loaded GG-GO-Fe_3O_4. The GG-GO-Fe_3O_4 nanocomposites had rod-like and spherical shapes, and the particles were distributed unevenly with sizes from 19.8 to 81.3 nm. Figure 4(c) shows that PEC-GO-Fe_3O_4 were spherical, with sizes between 8.43 and 15.4 nm. According to Ngenefeme *et al.* [21], the size distribution of the PEC-GO-Fe_3O_4 is reduced due to the presence of PEC, and the dispersion of magnetite contributed to less aggregation of the nanoparticles. Aggregation can still be observed as the coating of polymer on the GO-Fe_3O_4 nanocomposite is not uniform. Formation of core/shell particles which the GO-Fe_3O_4 cores are observable as a black area enclosed by a lighter grey shell were determined in both conjugated nanocomposites [22, 23]. This may allow for fine dispersion, high oxidation stability and improved drug loading on the shells.

In the context of loading cinnamaldehyde into PEC-GO-Fe_3O_4, the PEC-GO-Fe_3O_4 appears to be over-agglomerated (Figure 4(d)). After loading cinnamaldehyde, it is clear that the size of the PEC-GO-Fe_3O_4 was 2.3 to 5.6 times larger compared to empty PEC-GO-Fe_3O_4. As discussed by Ganguly and Pramanik [14], the agglomeration of PEC-GO-Fe_3O_4 is not favourable for drug delivery as it reduces the effective magnetisation, which may lead to a decline in drug delivery efficacy.

3.2 Reaction Mechanism

GO is an oxygen-rich material because it has covalently attached oxygen functional groups such as hydroxyl, epoxy, carbonyl and carboxyl groups. These functional groups can bind cinnamaldehyde and therefore will increase its solubility in water. In this research, two innovative strategies were entailed. Firstly, GO is functionalised with Fe_3O_4 to provide a magnetic property to GO in enhancing the ability of GO to bind and carry cinnamaldehyde. Secondly, the GO-Fe_3O_4 is conjugated with GG or PEC to prevent aggregation and increase the stability of the nanocomposite to load and release cinnamaldehyde.

This study involves three phases, namely synthesis of GO-Fe_3O_4, conjugation between biopolymers (GG and PEC) with GO-Fe_3O_4, and cinnamaldehyde loading into GG-GO-Fe_3O_4 and PEC-GO-Fe_3O_4 nanocomposites. Schematic diagrams on stages from the synthesis of nanocomposites to drug loading are illustrated in Figures 5(a) and (b). In this study, GO-Fe_3O_4 nanocomposites are prepared at 278 °C. In an environment of argon gas and high temperature, mixtures of iron acetylacetonate ($Fe(C_5H_7O_2)_3$) and graphene oxide (GO) are reacted in triethylene glycol. Under these conditions, decomposition of $Fe(C_5H_7O_2)_3$ to iron oxide (Fe_3O_4) occurred. In addition, Fe_3O_4 and GO interacted through ionic bond. According to Odularu [24], decomposition at high temperatures (>250 °C) can lead to a high production of small-size nanoparticles. In this study, the triethylene glycol used was a base (pH = 6.5–8.0) containing a high number of OH- ions. Triethylene glycol deprotonates the carboxylic acid and phenol groups of GO, leading to an abundance of negative charges in GO. Under these conditions, iron will potentially donate electrons

to GO and become attracted to carboxylic acid and phenol groups. This results in the formation of ionic bonds [25].

In the second phase, GG and PEC were conjugated with GO-Fe_3O_4. Theoretically, conjugation occurs during overlapping of *p* orbitals from adjacent atoms which can lead to stabilisation of molecules. Interactions between extra π-bonding and adjacent π systems of GG and PEC contribute to the stabilisation of the conjugate. The delocalisation of electrons in GG and PEC was affected by resonance and hybridisation energy [26]. The final phase was the entrapment of cinnamaldehyde into both GG-GO-Fe_3O_4 and PEC-GO-Fe_3O_4 nanocomposites. During the entrapment process, the hydroxyl group of cinnamaldehyde and hydrogen atoms of the nanocomposites led to hydrogen bonding. In this phase, the negative dipole of the hydrophobic drug was attracted by the positive dipole from the nanocomposites.

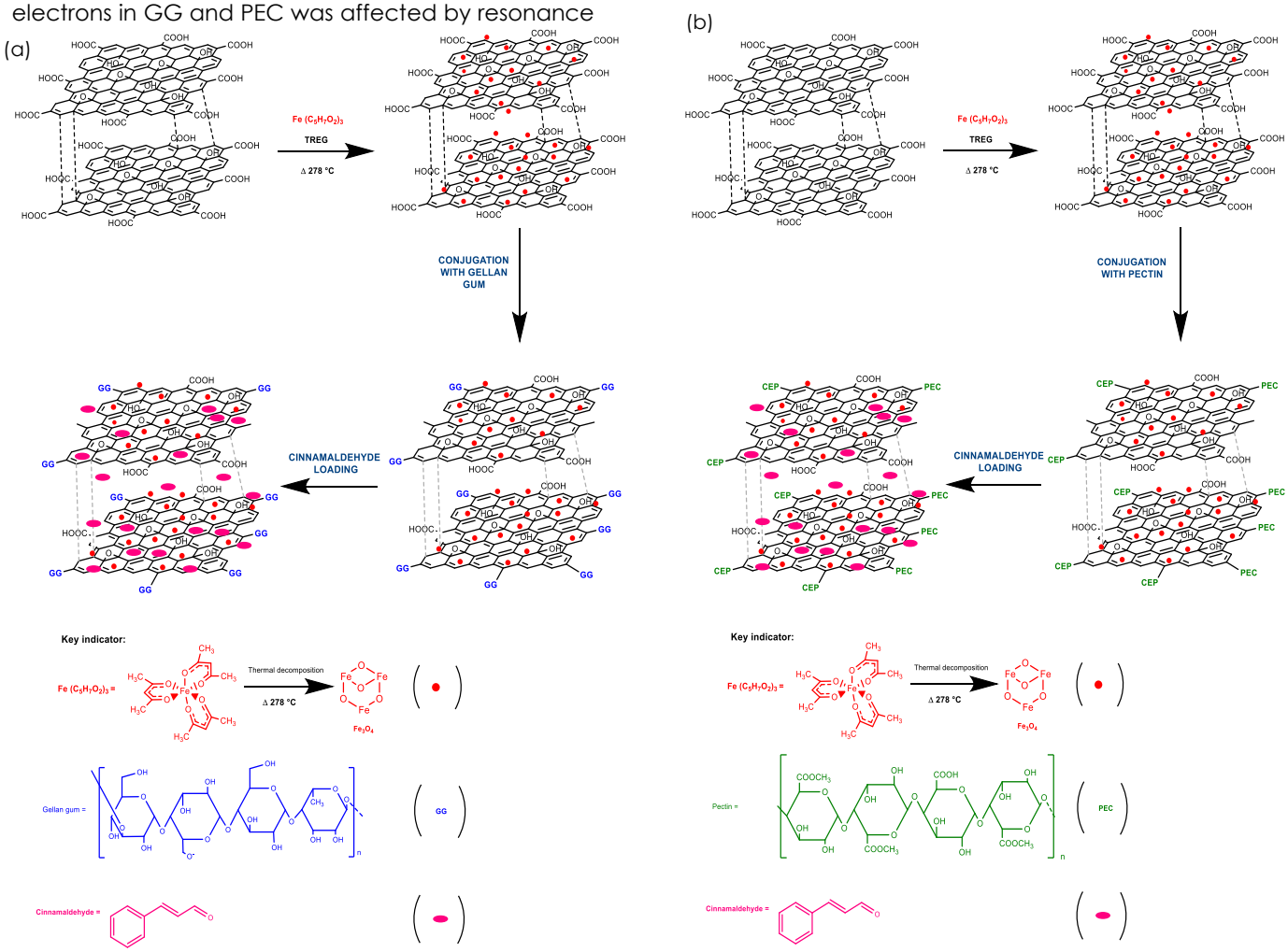

Figure 5 (a) Schematic diagram of preparation of GO-Fe_3O_4, GG-GO-Fe_3O_4 and cinnamaldehyde loaded GG-GO-Fe_3O_4 and (b) Schematic diagram of preparation of GO-Fe_3O_4, PEC-GO-Fe_3O_4 and cinnamaldehyde loaded PEC-GO-Fe_3O_4

3.3 Cinnamaldehyde-Loading Study

The cinnamaldehyde-loading profiles of GG-GO-Fe_3O_4 and PEC-GO-Fe_3O_4 nanocomposites are given in Table 1. The entrapment efficiencies of GG-GO-Fe_3O_4 at 1:5, 1:15 and 1:25 ratios (v/w, cinnamaldehyde to GG-GO-Fe_3O_4) reached 50.76%, 65.12% and 87.43%, respectively, and an increment is observed as the volume-to-weight ratio of the nanocomposites increases from 1:5 to 1:25. Meanwhile, the entrapment efficiencies of PEC-GO-Fe_3O_4 exhibit the same trend with the incremental increase of volume-to-weight ratio of the nanocomposites, but with a lower percentage increase. The PEC-GO-Fe_3O_4 nanocomposites in ratios of 1:5, 1:15 and 1:25 (v/w, cinnamaldehyde to GG-GO-Fe_3O_4) successfully entrapped 41.98%, 54.88% and 72.98% of the cinnamaldehyde, respectively.

Next, the evaluation about loading capacities were also conducted on both nanocomposites. The arrays of loading capacities for GG-GO-Fe_3O_4 and PEC-GO-Fe_3O_4 nanocomposites are 40.33% to 80.46% and 35.00% to 69.45%, respectively. These results confirm the increase in the number of reaction sites towards cinnamaldehyde in the nanocomposites. From Table 1, it is clear that the nanocomposite with a

volume-to-weight ratio of 1:25 had the highest EE and LC, due to an increase in the availability of reaction sites and surface area of the nanocomposites. It is obvious that GG-GO-Fe_3O_4 has higher EE and LC as compared to PEC-GO-Fe_3O_4 mainly because it has more available hydrogen atoms that could contribute to formation of hydrogen bonding with OH active sites of cinnamaldehyde molecules (Figure 5), as mentioned in Section 3.2.

There are several studies directed towards the construction of biopolymers with magnetic nanoparticles for the formation of new drug carriers for hydrophobic drugs. Although direct comparison on EE and LC studies from other researchers is not compatible, but it is crucial to highlight information on successful entrapment studies of hydrophobic drugs in biopolymer with magnetic drug system. For example, Ding *et al.* [27] synthesised chitosan-crosslinked carboxymethyl β-cyclodextrin–modified Fe_3O_4 magnetic nanoparticles to encapsulate the hydrophobic anticancer agent 5-flurouracil, in a ratio of 15:1:2 of chitosan:5-fluorouracil:carboxymethyl β-cyclodextrin, achieving 97.6 ± 1.3% EE. A type of polyethylene glycol (PEG)–modified liposome (PEGylated magnetic liposomes) synthesised by Hardiansyah *et al.* [28] encapsulated 76.15 ± 1.6% of curcumin. Muhoza *et al.* [29] synthesised microcapsules by way of coacervation between gelatin and methylated pectin to encapsulate cinnamaldehyde, and the EE of methylated pectin was reported in the range of 85.2 to 89.2%. Cinnamaldehyde can also be encapsulated by other types of nanoparticles. For instance, sodium alginate/chitosan nanocomposites were used to encapsulate 72.92% of cinnamaldehyde by Ji *et al.* [30].

Table 1 Entrapment efficiencies and loading capacities of cinnamaldehyde onto nanocomposites at different mass ratios (cinnamaldehyde:nanocompsosites)

Nanocomposite	Cinnamaldehyde: Nanocomposite	Entrapment efficiency (%)	Loading capacity (%)
GG-GO- Fe_3O_4	1:5	50.76 ± 0.15	40.33 ± 0.24
	1:15	65.12 ± 0.34	59.14 ± 0.35
	1:25	87.43 ± 0.44	80.46 ± 0.47
PEC-GO-Fe_3O_4	1:5	41.98 ± 0.23	35.00 ± 0.15
	1:15	54.88 ± 0.56	47.65 ± 0.28
	1:25	72.98 ± 0.79	69.45 ± 0.29

Values represent mean of three replicates ± standard deviation.

3.4 Cinnamaldehyde Release Study

The release behaviour of cinnamaldehyde from GG-GO-Fe_3O_4 and PEC-GO-Fe_3O_4 in rainwater at several mass ratios are shown in Figure 6. The drug release of all conjugated nanocomposites performed two-phase release profile, wherein burst release effect was observed before sustained drug release. The observed initial rapid release is due to the drug release from those trapped on the surface of conjugated nanocomposites [31]. Besides, the burst release may be caused by drug migration during the drying process, resulted in an uneven distribution of the drug in the conjugated GO-Fe_3O_4. The London dispersion forces and polarisability may contribute to stronger interactions between polymer chains and larger ions. The cinnamaldehyde release is restricted by entanglement from GG and PEC, therefore the release rates became slow after the burst release effect [32, 33].

The maximum absorbance of cinnamaldehyde was detected at 298 nm by the UV-Vis spectrophotometer. Cinnamaldehyde required only 52 h to achieve full release. After cinnamaldehyde loading, GG-GO-Fe_3O_4 with different volume-to-weight ratios showed a prolonged release of cinnamaldehyde over 36 h, as illustrated in Figure 6(a)(i). Meanwhile, the PEC-GO-Fe_3O_4 composite was able to prolong cinnamaldehyde release up till 76 h. The graphs for drug release of PEC-GO-Fe_3O_4 at the mass ratios of cinnamaldehyde:PEC-GO-Fe_3O_4 at 1:5, 1:15, and 1:25 are plotted in Figure 6(b). In a report by Ganguly and Pramanik [14], PEC-GO-Fe_3O_4 was synthesised for anticancer agent loading, namely curcumin, for targeted drug delivery. The curcumin released from the PEC-GO-Fe_3O_4 composite worked well in neutral and alkaline pH ranges, as the desired target drug release occurs in the large intestine and colon.

Studying drug release kinetics requires the application of mathematical models to approximate drug release processes and their behaviours. There are several release kinetic models, including zero-order, first-order, Higuchi, Korsmeyer-Peppas and Wiebull equations, for studying the release kinetics of compounds from sample materials. Table 2 presents

the release kinetic mechanism models for GG-GO-Fe_3O_4 and PEC-GO-Fe_3O_4 after cinnamaldehyde loading. The experimental data were best suited with Korsmeyer-Peppas models (R^2 values ranged from 0.9809 to 0.9965). The value of *k* can be varied based on the shape of nanocomposites. The shape of the polymer matrix (rod-like, spherical or film) is taken into consideration for the release curve of the Korsmeyer-Peppa kinetic model. For example, *n* of spherical particles is 0.42 for the mechanism that controlled by diffusion [34]. As discussed earlier, it was observed from STEM analysis that the GG-GO-Fe_3O_4 and PEC-GO-Fe_3O_4 nanocomposites possess spherical shapes (Figures 4(b) and (d)).

In this study, the consideration of *n* for spherical nanocomposites was applied. A Fickian diffusion release mechanism for the nanocomposite is indicated when *n* is less than 0.45. When the value of *n* is in the range of 0.45 to 0.85, the release mechanism is governed by anomalous transport. As mentioned earlier, the value of *n* exceeds 0.85 is an indicator for a Case II release mechanism to take place. The values of *n* obtained in this study are between 0.43 and 0.85, suggesting non-Fickian diffusion at play during the drug release. This indicates that the release of cinnamaldehyde from both nanocomposites obeys the anomalous transport mechanism. Işiklan and Polat [22] stated that non-Fickian diffusion of drugs means that the release of cinnamaldehyde is controlled by both processes of drug diffusion and stress relaxation of copolymers.

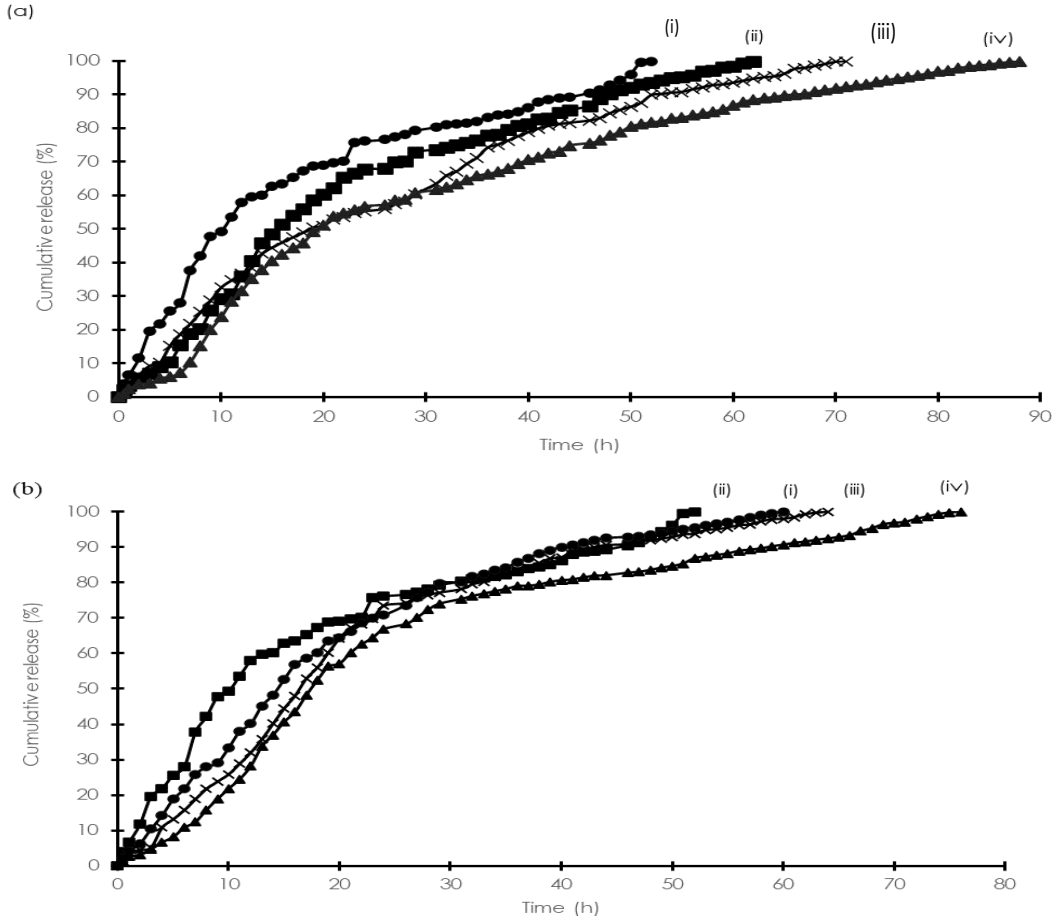

Figure 6 (a) Release profiles of (i) cinnamaldehyde, cinnamaldehyde loaded at the ratio of (ii) 1:5, (iii) 1:15 and (iv) 1:25 for GG-GO-Fe_3O_4 and (b) Release profiles of (i) cinnamaldehyde, cinnamaldehyde loaded at the ratio of (ii) 1:5, (iii) 1:15 and (iv) 1:25 for PEC-GO-Fe_3O_4

Table 2 R^2 and *n* values of kinetic models for cinnamaldehyde release from nanocomposites at different mass ratios

Cinnamaldehyde: Nanocomposites	Cinnamaldehyde loaded GG-GO-Fe_3O_4					Cinnamaldehyde loaded PEC-GO-Fe_3O_4				
	Zero-order	First-order	Higuchi	Korsmeyer-Peppas		Zero-order	First-order	Higuchi	Korsmeyer-Peppas	
	R^2	R^2	R^2	R^2	*n*	R^2	R^2	R^2	R^2	*n*
1:5	0.8233	0.7834	0.7654	0.9913	0.8734	0.9345	0.9312	0.9542	0.9822	0.8342
1:15	0.7754	0.7045	0.8054	0.9834	0.7833	0.8923	0.8094	0.8234	0.9965	0.8243
1:25	0.8982	0.9745	0.7546	0.9947	0.6234	0.9544	0.9643	0.8745	0.9809	0.6577

3.5 Larvicidal Studies

The discovery of a new, environmentally friendly nanocarrier for carrying larvicides is important to reduce the excessive usage and negative impacts of chemical insecticides in the environment. In this study, the effectiveness of nanocomposites was evaluated in the *A. aegypti* 4th instar larvicidal study. The ultimate goal of this experiment was to evaluate the efficacy of GO-Fe_3O_4 as nanocarriers for cinnamaldehyde in rainwater environments. The relationship between dose and the quantal response is investigated by using Probit analysis. In principle, the target species will be exposed to a specific drug at different concentrations in the quantal response experiment and the mortality percentage at each concentration recorded. Probit analysis provides the strength of a stimulus required in order to achieve a certain proportion of responses, such as median lethal dose [35].

During the larvicidal study, it was found that both cinnamaldehyde-unloaded nanocomposites from toxicity control test did not show any toxicity effect to *A. aegypti* mosquito larvae. Furthermore, the larvae from negative control group have been developed as adult mosquitoes after 78 h by observing the emergence of mosquitoes and pupal moulting on the water surface. After exposure to commercial temephos for 72 h, a 100-mortality rate is discovered. Temephos has been widely used in vector management, particularly for mosquito larvae control in Malaysia since 1970. According to Thavara *et al.* [36], the effectiveness of temephos in water storage containers towards *A. aegypti* mosquitoes can last for two to three months. However, if there is any dilution or removal of water, the efficacy may decrease. In last few years, various researchers reported on the resistance of mosquito larvae towards temephos [37-39]. Since 1987, researchers have increased the dosage of temephos to control mosquito larvae, which may have increased the resistance level of the larvae towards temephos. The WHO-recommended dosage of temephos is 0.012 mg/L but Multyano *et al.* [38] have reported that larvae in Indonesia were not susceptible to this dosage of temephos.

Table 3. Effectiveness of cinnamaldehyde loaded nanocomposites towards *A. aegypti* larvae

Exposure time	GG-GO-Fe_3O_4			PEC-GO-Fe_3O_4		
	24 h	**48 h**	**72 h**	**24 h**	**48 h**	**72 h**
LC_{50} (mg/L) (Confidence limit 95%)	6.02 (4.83-7.22)	5.85 (4.86-6.84)	3.40 (2.04-4.75)	14.63 (13.96-15.91)	4.60 (3.39-5.80)	3.83 (2.25-5.42)
Percentage mortality (%)	53.28	66.66	86.58	33.33	46.62	69.93
Probit equation	3.1916 + 2.3195x	2.3355 + 3.4733x	3.7462 + 2.3601x	2.6229 + 2.0398x	4.2437 +1.1414x	1.8772 + 5.3504x
Standard error	1.1955	1.2520	1.3534	0.9782	1.2060	1.5877
R^2	0.9779	0.8979	0.9576	0.9967	0.8903	0.9535

The value of LC_{50} can be obtained from log Probit analysis. As the value of LC_{50} increases, higher concentrations are required to achieve 50% mortality of the organisms, and this stipulated that the less toxic the chemical would be. The results of this analysis and the lower and upper limit ranges of toxicity are shown in Table 3. It is clear that LC_{50} showed a decline trend in concentration every 24 h. It is noted that same mortality occurs at 24 and 48 h, although the median lethal concentration is reduced. The mortality percentage is not as high as cinnamaldehyde-loaded GG-GO-Fe_3O_4 and this may be due to the amount of encapsulated cinnamaldehyde in the PEC-GO-Fe_3O_4 being lower than in GG-GO-Fe_3O_4, and the cinnamaldehyde released is insufficient to achieve 100% mortality. As discussed for findings from Section 2.2 (Cinnamaldehyde-loading studies), the PEC-GO-Fe_3O_4 entrapped 41% to 72% of cinnamaldehyde, and the EE of GG-GO-Fe_3O_4 achieves 50% to 87% of the cinnamaldehyde concentration, and the mortality rate is much stronger than GG-GO-Fe_3O_4, as shown by the R^2 values exceeds 0.8900.

From these results, it can be concluded that GG-GO-Fe_3O_4 is a better nanocarrier than PEC-GO-Fe_3O_4 for cinnamaldehyde as it prolongs the release of cinnamaldehyde for a longer time period. An ideal nanocarrier reduces the necessary amounts of drugs required for entrapment in order to achieve efficient drug delivery [40].

4.0 CONCLUSION

The conjugated magnetic graphene oxide nanocomposites possess good EE and LC values, making them ideal nanocarriers for cinnamaldehyde. The use of GG-GO-Fe_3O_4 and PEC-GO-Fe_3O_4 nanocomposites as water solubilising agents has successfully increased the solubility of cinnamaldehyde in water by 35.9 and 29.6 times,

respectively. GG-GO-Fe_3O_4 nanocomposites exhibited superior EE and LC values, as compared to PEC-GO-Fe_3O_4 nanocomposites. The release of cinnamaldehyde from magnetic nanocomposites into rainwater followed a non-Fickian diffusion mechanism and was prolonged over 36 h. Compared with temephos, a commercial larvicide, GG-GO-Fe_3O_4 nanocomposites achieved 87.57% of the same mortality percentage with an LC_{50} of only 3.3982 mg/L. The effectiveness of GG-GO-Fe_3O_4 and PEC-GO-Fe_3O_4 nanocomposites to control *A. aegypti* larvae was comparable to that of temephos, with mortality percentages of 87.57%, 68.88% and 100.00%. Thus, the cinnamaldehyde-loaded conjugated magnetic graphene oxide nanocomposites may be considered for the effective application of larvicide formulations in future.

Conflicts of Interest

The author(s) declare(s) that there is no conflict of interest regarding the publication of this paper.

Acknowledgement

We thank Ministry of Higher Education Malaysia for providing a financial support (FRGS 2021-0188-103-02).

References

[1] World Health Organization (WHO). 2021, October 14. *Zika Virus Disease-India.* https://www.who.int/emergencies/disease-outbreak- news/item/zika-virus-disease-india.

[2] World Health Organization (WHO). 2022, January 10. *Dengue and Severe Dengue*. https://www.who.int/news-room/fact-sheets/detail/dengue-and-severe-dengue.

[3] World Health Organization (WHO): Western Pacific Region. 2023, March 30. *Dengue Situation Update 668.* https://www.who.int/westernpacific/emergencies/surveillance/dengue.

[4] European Centre for Disease Prevention and Control (ECDC). 2023, March 17. *Dengue Worldwide Overview*. https://www.ecdc.europa.eu/en/dengue-monthly.

[5] Ahmad, R., Suzilah, I., Najdah, W. M. A. W., Topek, O., Mustafakamal, I. and Lee, H. L. 2018. Factors Determining Dengue Outbreak in Malaysia. *PLOS One*. 13: e0193326. Doi: https://doi.org/10.1371/journal.pone.0193326.

[6] World Health Organization (WHO). 2013. *Larval Source Management: A Supplementary Measure for Malaria Vector Control: An Operational Manual.* https://apps.who.int/iris/bitstream/handle/10665/85379/9789241 505604_eng.pdf.

[7] Cheng, S. S., Huang, C. G., Chen, Y. J., Yu, J. J., Chen, W. J. and Chang, S. T. 2009. Chemical Compositions and Larvicidal Activities of Leaf Essential Oils from Two *Eucalyptus* Species. *Bioresource Technology*. 100(1): 452-456. Doi: https://doi.org/10.1016/j.biortech.2008.02.038.

[8] Wong, S. T. S., Kamari, A., Jaafar, A., Hussien, M., Othman, H., Abdullah, H., Yusof, N. and Hashim, N. 2020. Longer Mosquito Control Using a Sodium Alginate-Chitosan Nanocarrier for Cinnamaldehyde in Larvicide Formulations. *Environmental Chemistry Letters*. 18: 1345-1351. Doi: http://dx.doi.org/10.1007/s10311-020-00993-z.

[9] Hussien, N. A., Işiklan, N and Türk, M. 2018. Pectin-Conjugated Magnetic Graphene Oxide Nanohybrid as A Novel Drug Carrier for Paclitaxel Delivery. *Artificial Cells, Nanomedicine, and Biotechnology*. 46(1): 264-273. Doi: https://doi.org/10.1080/21691401.2017.1421211.

[10] Wang, L., Lai, S-Y., Li, C-Z., Yu, H-P., Venkatesan, P. and Lai, P-S. 2022. D-Alpha-Tocopheryl Poly(ethylene Glycol 1000) Succinate-Coated Manganese-Zinc Ferrite Nanomaterials for a Dual-Mode Magnetic Resonance Imaging Contrast Agent and Hyperthermia Treatments. *Pharmaceutics.* 14(5): 1000. Doi: https://doi.org/10.3390/pharmaceutics14051000.

[11] Guo, J., Giusti, M. M. and Kalentunç, G. 2018. Encapsulation of Purple Corn and Blueberry Extracts in Alginate-Pectin Hydrogel Particles: Impact of Processing and Storage Parameters on Encapsulation Efficiency. *Food Research International*. 107: 414-422. Doi: https://doi.org/10.1371/journal.pone.0112975

[12] Ritger, P. L. and Peppas, N. A. 1987. Simple Equation for Description of Solute Release Ii. Fickian and Anomalous Release from Swellable Devices. *Journal of Controlled Release*. 5(1): 37-42. Doi: https://doi.org/10.1016/0168-3659(87)90035-6.

[13] Finney, D. J. 1952. *Probit Analysis: A Statistical Treatment of the Sigmoid Response Curve*. Cambridge: Cambridge University Press.

[14] Ganguly, M. and Pramanik, D. 2017. Pectin Coated Iron Oxide Nanocomposite - A Vehicle for Controlled Release of Curcumin. *International Journal of Biology and Biomedical Engineering*. 11: 143-160.

[15] Stuart, B. 2021. Analytical Techniques in Forensic Science. In *Infrared Spectroscopy*. New Jersey: John Wiley & Sons Ltd. 145-160.

[16] Kumari, K. and Ramakrishnan, V. 2023. Fourier Transform Infrared (FTIR) Spectroscopy. In: Ramakrishnan, V. (eds). *Biophysical Characterization of Functional Peptides*. New York: Springer Protocols. 51-54. Doi: https://doi.org/10.1007/978-1-0716-3405-9_7.

[17] Balachandramohan, J., Anandan, S. and Sivasankar, Y. 2017. A Simple Approach for the Sonochemical Synthesis of Fe_3O_4-guargum Nanocomposite and Its Catalytic Reduction of p-nitroaniline. *Ultrasonic Sonochemistry*. 40(A): 1-10. Doi: https://doi.org/10.1016/j.ultsonch.2017.06.012.

[18] Zhu, W., Wu, J., Guo, X., Sun, X., Li, Q., Wang, J. and Chen, L. 2020. Development and Physicochemical Characterization of Chitosan Hydrochloride/Sulfobutyl Ether-β-Cyclodextrin Nanoparticles for Cinnamaldehyde Entrapment. *Journal of Food Biochemistry*. 44(6): e13197. Doi: https://doi.org/10.1111/jfbc.13197.

[19] Shahin, L., Zhang, L., Mohnen, D., Urbanowicz, B. R. 2023. Insights into Pectin *O*-Acetylation in the Plant Cell Wall: Structure, Synthesis, and Modification. *The Cell Surface*. 9: 100099. Doi: https://doi.org/10.1016%2Fj.tcsw.2023.100099.

[20] Ghibaudo, F., Gerbino, E., Copello, G.J., Dall'Orto, V. V. and Gómez-Zavaglia, A. 2019. Pectin-decorated Magnetite Nanoparticles as Both Iron Delivery Systems and Protective Matrices for Probiotic Bacteria. *Colloids and Surfaces B: Biointerfaces*. 180: 193-201. Doi: https://doi.org/10.1016/j.colsurfb.2019.04.049.

[21] Ngenefeme, F. J., Eko, N. J., Mbom, Y. D., Tantoh, N. D. and Rui, K. W. M. A. 2013. One Pot Green Synthesis and Characterisation of Iron Oxide-Pectin Hybrid Nanocomposite. *Open Journal of Composite Materials*. 3(2): 30-37. Doi: http://dx.doi.org/10.4236/ojcm.2013.32005.

[22] Işiklan, N. and Polat, S. 2020. Synthesis and Characterization of Thermo/pH-Sensitive Pectin-Graft-Poly (Dimethylaminoethyl Methacrylate) Coated Magnetic Nanoparticles. *International Journal of Biological Macromolecules*. 164: 4499-4515. Doi: https://doi.org/10.1016/j.ijbiomac.2020.09.002.

[23] Ebadi, M., Zain, A. R. M., Aziz, T. H. T. A., Mohammadi, H., Lee, C. A. T. H. and Yusop, M. R. 2023. Formulation and Characterization of Fe_3O_4@PEG Nanoparticles Loaded Sorafenib; Molecular Studies and Evaluation of Cytotoxicity in Liver Cancer Cell Lines. *Polymers*. 15(4): 971. Doi: https://doi.org/10.3390/polym15040971.
[24] Odularu, A. T. 2018. Metal Nanoparticles: Thermal Decomposition, Biomedicinal Applications to Cancer Treatment, and Future Perspectives. *Bioinorganic Chemistry and Applications*. 2018: 9354708. Doi: https://doi.org/10.1155/2018/9354708.
[25] Trivedi, V. 2019. *Chemical Bonding for JEE Main & Advanced, NEET*. 2nd edition. New Delhi: Disha Publication.
[26] Ali, H. 2016. *Reaction Mechanism in Organic Chemistry*. New Delhi: S. Chand and Company Limited.
[27] Ding, Y., Shen, S. Z., Sun, H., Sun, K., Liu, F., Qi, Y. and Yan, J. 2015. Design and Construction of Polymerized-Chitosan Coated Fe_3O_4 Magnetic Nanoparticles and Its Application for Hydrophobic Drug Delivery. *Materials Science and Engineering: C*. 48: 487-498. Doi: https://doi.org/10.1016/j.msec.2014.12.036.
[28] Hardiansyah, A., Yang, M.C., Liu, T. Y., Kuo, C. Y., Huang, L. Y. and Chan, T. Y. 2017. Hydrophobic Drug-Loaded PEGylated Magnetic Liposomes for Drug-Controlled Release. *Nanoscale Research Letters*. 12(1): 355. Doi: https://doi.org/10.1186/s11671-017-2119-4.
[29] Muhoza, B., Xia, S., Cai, J., Zhang, X., Duhoranimana, E. and Su, J. 2019. Gelatin and Pectin Complex Coacervates as Carriers for Cinnamaldehyde: Effect of Pectin Esterification Degree on Coacervate Formation, and Enhanced Thermal Stability. *Food Hydrocolloids*. 87: 712-722. Doi: https://doi.org/10.1016/j.foodhyd.2018.08.051.
[30] Ji, M., Sun, X., Guo, X., Zhu, W., Wu, J., Chen, L., Wang, J., Chen, M., Cheng, C. and Zhang, Q. 2019. Green Synthesis, Characterization and *In Vitro* Release of Cinnamaldehyde/Sodium Alginate/Chitosan Nanoparticles. *Food Hydrocolloids*. 90: 515-522. Doi: https://doi.org/10.1016/j.foodhyd.2018.12.027.
[31] Supramaniam, J., Adnan, R., Kaus, N. H. M. and Bushra, R. 2018. Magnetic Nanocellulose Alginate Hydrogel Beads as Potential Drug Delivery System. *International Journal of Biological Macromolecules*. 118(A): 640-648. Doi: https://doi.org/10.1016/j.ijbiomac.2018.06.043.
[32] Bernasconi, R., Pizzetti, F., Rosseti, A., Perugini, R., Nova, A., Levi, M. and Rossi, F. 2021. Effect of Different Physical Cross-Linkers on Drug Release from Hydrogel Layers Coated on Magnetically Steerable 3D-Printed Microdevices. *Technologies*. 9(2): 43. Doi: https://doi.org/10.3390/technologies9020043.
[33] Das, S., Thomas, S and Das, P. P. 2023. *Novel Platforms for Drug Delivery Applications*. Cambridge: Woodhead Publishing (Elsevier Ltd). Doi: https://doi.org/10.1016/C2020-0-04022-3.
[34] Varga, N., Turcsányi, Á., Hornok, V. and Csapó, E. 2019. Vitamin E-Loaded PLA- and PLGA-Based Core-Shell Nanoparticles: Synthesis, Structure Optimization and Controlled Drug Release. *Pharmaceutics*. 11(7): 0357. Doi: https://doi.org/10.3390/pharmaceutics11070357.
[35] Barkai-Golan, R. and Follett, P. A. 2017. Phytosanitary Irradiation of Fresh Horticultural Commodities for Market Access. *Irradiation for Quality Improvement, Microbial Safety and Phytosanitation of Fresh Produce*. London: Elsevier Ltd. 171-190.
[36] Thavara, U., Tawatsin, A., Kong-Ngamsuk, W. and Mulla, M. S. 2004. Efficacy and Longevity of a New Formulation of Temephos Larvicide Tested in Village-Scale Trials Against Larval *Aedes aegypti* In Water-Storage Containers. *Journal of the American Mosquito Control Association*. 20(2): 176-182.
[37] Vasantha-Srinivasan, P., Senthil-Nathan, S., Ponsankar, A., Thanigaivel, A., Edwin, E., Selin-Rani, S., Chellappandian, M., Pradeepa, V., Lija-Escaline, J., Kalaivani, K., Hunter, W. B., Duraipandiyan, V. and Al-Dhabi, N. A. 2017. Comparative Analysis of Mosquito (Diptera: Culicidae: *Aedes aegypti Liston*) Responses to the Insecticide Temephos And Plant Derived Essential Oil Derived From *Piper betle L. Ecotoxicology and Environmental Safety*. 139: 439-446. Doi: https://doi.org/10.1016/j.ecoenv.2017.01.026.
[38] Multyano, K. C., Yamanaka, A. and Ngadino Konishi, E. 2012. Resistance of *Aedes aegypti* (L.) Larvae to Temephos in Surabaya, Indonesia. *The Southeast Asian Journal of Tropical Medicine and Public Health*. 43(1): 29-33.
[39] Wan-Norafikah, O., Aliah-Diyanah, S., Atiqah-Izzah, Z., Chen C. D., Sofian-Azirun, M., Lailatul-Nadhirah, A., Ibahim, M. J. 2023. Assessing the Bioefficacy of a Commercial Temephos Formulation (Temebate®) for Controlling *Aedes albopictus* Larvae in Different Land Use Localities in Malaysia. *Experimental Parasitology*. 254: 108627. Doi: https://doi.org/10.1016/j.exppara.2023.108627.
[40] Patra, J. K., Das, G., Fraceto, L. F., Campos, E. V. R., del Pilar Rodriguez-Torres, M., Acosta-Torres, L. S., Diaz-Torres, L. A., Grillo, R., Swamy, M. K., Sharma, S., Habtemariam, S. and Shin, H. S. 2018. Nano Based Drug Delivery Systems: Recent Developments and Future Prospects. *Journal of Nanobiotechnology*. 16: 71. Doi: https://doi.org/10.1186/s12951-018-0392-8.